UNIVERSIDADE D
COIMBRA

Alexandre Pereira Ganhito

MODELING A SOLID PROPELLANT ROCKET ON A VERTICAL TRAJECTORY IN THE EARTH'S ATMOSPHERE

Dissertação no âmbito do Mestrado em Engenharia Mecânica, na Especialidade de Energia e Ambiente, orientada pelo Professor Doutor Pedro de Figueiredo Vieira Carvalheira, apresentada ao Departamento de Engenharia Mecânica da Faculdade de Ciências e Tecnologia da Universidade de Coimbra.

Setembro de 2023

FACULDADE DE CIÊNCIAS E TECNOLOGIA
UNIVERSIDADE D COIMBRA

Modeling a Solid Propellant Rocket on a Vertical Trajectory in the Earth's Atmosphere

A dissertation submitted in partial fulfilment of the requirements for the degree of Master in Mechanical Engineering in the specialty of Energy and Environment.

Modelação de um Foguete de Propergol Sólido numa Trajetória Vertical na Atmosfera Terrestre

Author

Alexandre Pereira Ganhito

Advisor

Pedro de Figueiredo Vieira Carvalheira

Committee

Chair	**Professor Doutor Almerindo Domingues Ferreira** **Professor Auxiliar da Universidade de Coimbra**
Member	**Professor Doutor José Manuel Baranda Moreira da Silva Ribeiro** **Professor Associado da Universidade de Coimbra**
Advisor	**Professor Doutor Pedro de Figueiredo Vieira Carvalheira** **Professor Auxiliar da Universidade de Coimbra**

Coimbra, September 2023

ACKNOWLEDGEMENTS

The work presented in this thesis would not be possible without the valuable contribution of my advisor, Professor Pedro de Figueiredo Vieira Carvalheira, for the availability always demonstrated, mentorship and the shared knowledge.

His expertise in this field has provided me with valuable insights and shaped the content and direction of this thesis.

I would like to express my gratitude to my family for all the support and belief they have placed in me throughout my academic journey, for all my educational experiences before I enrolled here, as well as for all the opportunities and good things I've experienced throughout my life.

I would also like to thank the entire academic community, with a special note of gratitude to my closest friends throughout the years, for sharing in all the positive academic experiences as well as the struggles of a student life.

Finally, I would like to express my gratitude to the academic institution, University of Coimbra, and in particular, the Department of Mechanical Engineering, for providing all the comfort and means to my success, as well as all the professors I've had the privilege to learn from during my studies.

Abstract

The main objective of the work presented is the development of a model to simulate the motion of a rocket propelled by a solid propellant rocket motor in the Earth's atmosphere, in a vertical trajectory.

The model also simulates the operating parameters of the rocket motor, as well as the interaction of the rocket with the earth's atmosphere by means of the calculations of aerodynamic drag, and the evolution of the vehicle mass because of the solid propellant burning.

To make this possible, it is first created a model of the Earth's atmosphere that allows us to calculate all its relevant properties in the range of altitudes of interest for this study.

This model is created in MATLAB, and the differential equations that model the rocket motion and rocket motor operation are solved by the Euler method.

The model created is used to describe the motion of a rocket based on the Rexus-10, from ESA, for which there's sufficiently detailed information available for validation of the simulation results.

The model created is used to optimize the effect of the nozzle throat diameter of the rocket motor on the apogee altitude of the rocket flight. Using the model created simulations are made where the only variable changed between simulations is the nozzle throat diameter of the rocket motor, incremented by an appropriate value for the study of that parameter between two limiting values of interest.

It is also analyzed the impact that the payload carried by the rocket has in its apogee altitude, using a set of simulation results in which the payload is the only variable changed between each simulation.

The results of the simulation are ultimately compared with the experimental results of the ESA's Rexus-10 rocket available in the literature.

Keywords: Rocket, Rocket Motor, Composite Solid Propellant, Motion Modeling, Ammonium Perchlorate, Burning Characteristics.

Resumo

O principal objetivo do trabalho apresentado é o desenvolvimento de um modelo para simular o movimento de um foguete propulsionado por um motor foguete de propergol sólido na atmosfera terrestre, em trajetória vertical

O modelo também simula os parâmetros de operação do motor foguete, bem como a interação do foguete com a atmosfera terrestre, por meio do cálculo do arrasto aerodinâmico, bem como a evolução da massa do veículo, como resultado da queima do propergol sólido.

Para que isso seja possível, é primeiro criado um modelo da atmosfera terrestre que permite calcular as suas propriedades relevantes na faixa de altitudes de interesse para o nosso estudo.

Este modelo é criado em MATLAB, e as equações diferenciais que modelam o movimento do foguete e a operação do motor foguete são resolvidas através do método de Euler.

O modelo criado é usado para descrever o movimento de um foguete baseado no Rexus-10, da ESA, para o qual há informação suficientemente detalhada disponível para validar os resultados da simulação.

O modelo criado é utilizado para otimizar o efeito do diâmetro da garganta da tubeira do motor foguete na altitude de apogeu do vôo do foguete. Utilizando o modelo criado são feitas simulações onde a única variável alterada entre as simulações é o diâmetro da garganta da tubeira do motor foguete, incrementado por um valor apropriado para o estudo daquele parâmetro entre dois valores limites de interesse.

É também analisado o impacto que a carga útil transportada pelo foguete tem na sua altitude de apogeu, utilizando um conjunto de resultados de simulação em que a carga útil é a única variável alterada entre cada simulação.

Os resultados da simulação são finalmente comparados com os resultados experimentais do foguete Rexus-10 da ESA disponíveis na literatura.

Palavras-chave: Foguete, Motor Foguete, Propergol Sólido Compósito, Modelação do Movimento, Perclorato de Amónio, Características de Combustão.

Contents

LIST OF FIGURES

LIST OF TABLES

LIST OF SIMBOLS AND ACRONYMS/ ABBREVIATIONS

List of Symbols

a – Acceleration

A_b – Burning area of propellant grain

A_e – Cross-sectional area of the nozzle's exit

A_{fin} – Area of fin exposed to air flow

A_{fus} – Area of the fuselage exposed to air flow

A_t – Cross-sectional area of the nozzle's throat

C_p – Heat capacity at constant pressure

$C_{p,i}$ – Heat capacity at constant pressure of species *i* in the atmosphere

C_s – Speed of sound

C_v – Heat capacity at constant volume

C_x – Drag coefficient

d_b – Diameter of burning area

d_e – Diameter of the nozzle's exit

d_p – Diameter of propellant

d_{rm} – External diameter of rocket motor

D – Drag

g – Gravitational acceleration

H – Geopotential height

H_b – Geopotential height at subscript *b*

l_p – Length of propellant burning area

m – Mass of the rocket

m_{er} – Mass of empty rocket

m_p – Propellant mass

M_0 – Molecular mass of the atmosphere at zero altitude

Ma – Mach number

M_{air} – Molecular mass of air

M_b – Molecular mass of the propellant combustion products

n_i – Number density of species *i* in the atmosphere

P – Pressure

P_b – Pressure at subscript *b*

P_c – Chamber pressure

P_e – Nozzle's exit section pressure

r_0 – Earth's radius

r_p – Propellant burning rate

R^* – Ideal gas constant

Re_{fin} – Reynolds at the fins

Re_{fus} – Reynolds at the fuselage

S – Sutherland's constant

t – Time

t_0 – Initial time

T – Thrust

T_b – Flame temperature

T_k – Kinetic temperature of air in the earth's atmosphere

T_m – Molecular-scale temperature

v – Velocity

v_0 – Initial velocity

v_e – Flow velocity at the cross-sectional area of the nozzle's exit

W – Weight

x_i – Molar fraction of species *i* in the atmosphere

Z – Geometric height

μ – Dynamic viscosity

ρ_{air} – Density of air

ρ_p – Density of the propellant.

γ_{air} – Specific heat ratio of the atmosphere

γ_p – Specific heat ratio of the combustion products

Acronyms/Abbreviations

DEM – Departamento de Engenharia Mecânica

ESA – European Space Agency

FCTUC – Faculdade de Ciências e Tecnologia da Universidade de Coimbra

MATLAB – Matrix Laboratory

NASA – National Aeronautics and Space Administration

CEA – Chemical Equilibrium with Applications

DLR – German Aerospace Center

SNSA – Swedish National Space Agency

1. INTRODUCTION

1.1. Motivation

Rockets are devices of growing importance today, as they become more widely available for all types of research, as a result the need for a widespread database of investigation on their motion has more importance than ever.

Sounding rockets, with their swift ascent into the outer reaches of the atmosphere, serve as essential tools for probing Earth's atmosphere upper limits, conducting scientific experiments and testing new aerospace technologies.

The motivation behind this thesis is inspired by the convergence of scientific curiosity, technological advancement and the inherent thrill of space exploration.

With this research, I aim to contribute valuable information to a less widely known field of study. Much of the research in this area remains inaccessible to the public.

The hope is that the findings of this study will inspire innovation in the field of aeronautics. Scientific exploration using sounding rockets offers a range of benefits to modern society, including insights gained from atmospheric research, microgravity research, aurora and ionospheric studies, technology testing, particle and cosmic ray research, as well as magnetospheric studies.

Finally, the choice of this field of study was fueled by my own passion for aerospace exploration.

2. LITERATURE REVISION

2.1. Sounding Rockets

Sounding rockets are suborbital vehicles with the purpose of conducting experiments in a range of altitude that can go from 50 km to 750 km (Sounding rockets, 2023).

Their payload is usually experimental equipment designed to conduct the intended experiments.

They can be easily and affordably deployed into space, a capability that is not only crucial for time-sensitive research with a narrow window of opportunity for study, but also cost-effective, thus enabling a greater number of institutions to access such devices.

They are widely employed in various research areas, including the study of Earth's atmosphere, astronomy, physics, microgravity experiments and the development of experimental technologies.

2.2. Flight Motion

The flight motion of the rocket can be easily described by a few parameters, such as the mass, weight, thrust and drag in effect on the vehicle during its flight time.

The change in mass during our simulation is solely affected by the propellant mass burn rate and makes the full mass of the rocket decrease as time passes, until there’s no more propellant to burn, which is the moment that, in most cases, such as in our simulation, the mass becomes constant for the rest of the flight.

The rocket motor thrust is dependent on parameters such as the type of propellant, the geometry of the propellant grain inside the rocket motor and the diameter of the throat of the nozzle.

In the case of our study, we are using two different propellants in the rocket motor to achieve the desired flight curve, and we simulate the flight characteristics by changing the diameter of the nozzle’s throat to find out what is the ideal diameter.

The drag coefficient depends on the rocket's body shape, fins, ogive, and the nozzle diameter of the rocket motor at its exit section.

In the case of our rocket, we picked a fixed ogive geometry that we found to be the most adequate to our rocket and the intended characteristics of the flight.

Our rocket has three fins of fixed geometry and is based on the geometry of the fins in the Rexus-10 model.

In the case of the diameter at the exit of the nozzle, it is fixed to be the same diameter as the diameter at the rear end of the rocket's body, with the intent to optimize the drag coefficient in that section of the nozzle.

The forces acting on the rocket during its trajectory are represented on Figure 2.1.

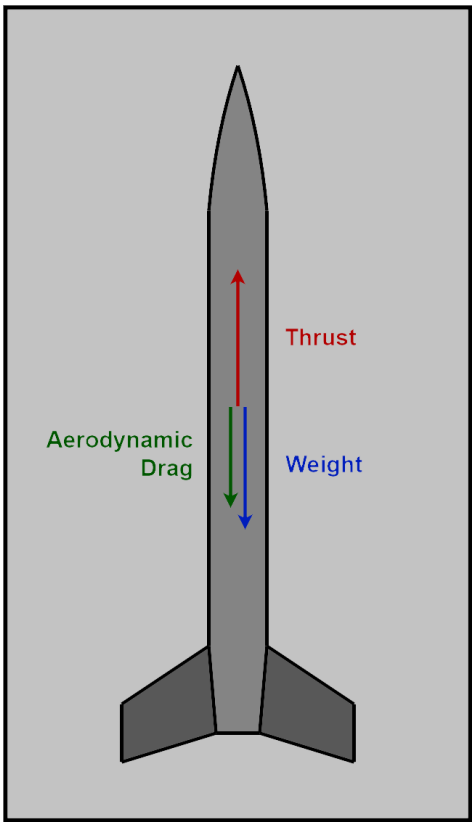

Figure 2.1. Diagram depicting the forces acting on the rocket during its trajectory.

2.3. Modeling the Rocket Motor

In the design of a model to emulate the flight properties of Rexus-10, it was decided that the rocket motor would be using two different propellants in a hollow cylinder made of two adjacent cylindrical layers of solid propellants, in which the inner layer is composed of propellant 1, that burns first and has a high burning rate, while the second propellant, which is in the outer layer and is composed of propellant 2, burns at a slower rate and is used to maintain a longer and more efficient thrust phase.

2.3.1. Solid Propellant Characteristics

The properties and chemical composition of both propellants are presented in Table 2.1, Table 2.2 and Table 2.3.

The properties in this table were obtained using the program CEA (Chemical Equilibrium with Applications) from NASA, which is a program that calculates chemical equilibrium products composition from any set of reactants and determines thermodynamic and transport properties for the products mixture.

Table 2.1. Properties of the propellants used in the rocket motor.

Properties	Propellant 1	Propellant 2
a $(\mathrm{mm} \cdot \mathrm{s}^{-1} \cdot \mathrm{MPa}^{-n})$	5.477	2.470
n	0.3852	0.4900
T_b (K)	3307.0	2363.7
M_b (kg/mol)	0.026983	0.022079
γ_p	1.1430	1.2372
ρ_p $(\mathrm{kg/m^3})$	1730.6	1587.6

Table 2.2. Chemical composition of propellant 1 in mass percentage

Chemical Composition	Propellant 1
AP 200 µm	48.30 %
AP 6 µm	20.70 %
HTPB	13.85 %
IPDI	1.15 %
Aluminum	16.00 %

Table 2.3. Chemical composition of propellant 2 in mass percentage

Chemical Composition	Propellant 2
AP 400 µm	40.00 %
AP 20 µm	40.00 %
HTPB	18.47 %
IPDI	1.53 %
Aluminum	0.00 %

2.4. Aerodynamic Drag

The aerodynamic drag is dependent on the rocket's shape, cross-sectional area, velocity, and is also dependent of the properties of the atmosphere, that change with altitude.

It is also dependent on the Re of the flow on the exposed surfaces and whether the flow around the rocket is subsonic, transonic or supersonic, which in the case of the ogive, is more accurately calculated based on experimental data.

Ultimately, the drag depends on whether the rocket is in the combustion phase; in this case, the drag related to the nozzle's exit cross-section is considered irrelevant.

2.5. Rocket Weight Modeling

The rocket weight is calculated using Eq. 2.1.

$$W = -m \cdot g \tag{2.1}$$

where W is the weight of the rocket in N, m is the mass of the rocket in kg, and g is the gravitational acceleration.

Both the mass of the rocket and gravity actuating on it will change during the flight, meaning that the weight will also have a variable instantaneous value.

The mass of the rocket is the sum of the mass of the structure, the rocket motor and its solid propellant, the capsule that protects the payload, and the payload itself.

In the case of our study, in each individual flight simulation, only the solid propellant mass will be changing during the flight, while the rocket payload will only change from one simulation to the other.

The gravitational acceleration will be only dependent of the altitude of the rocket, Z, based on Eq. 2.2 from NOAA (NOAA, NASA, & USAF, 1976), because the gravitational acceleration at altitude zero, g_0, is a constant and the Earth's radius, r_0, is also a constant.

$$g = g_0 \cdot \frac{{r_0}^2}{(r_0 + Z)^2} \tag{2.2}$$

Figure 2.2 describes the gravitational acceleration as a function of altitude.

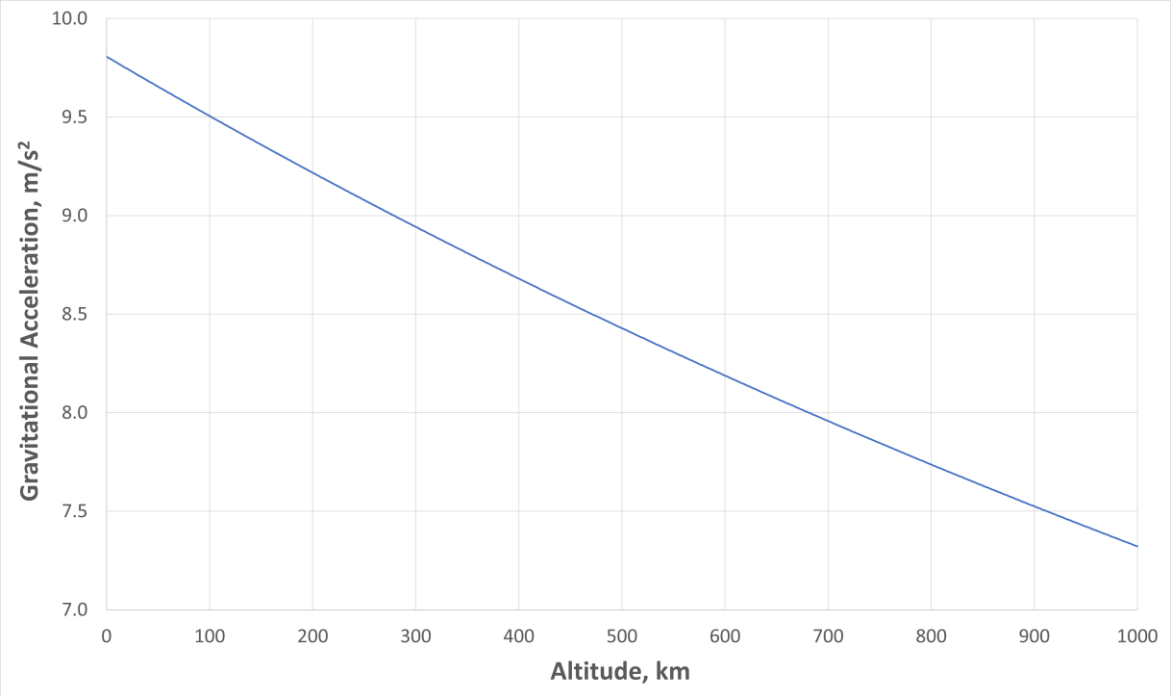

Figure 2.2. Gravitational acceleration as a function of altitude.

3. COMPOSING OF THE SIMULATION IN MATLAB

The differential equations used in the simulation of the rocket and rocket motor were solved using the Euler method to calculate the changes in multiple variables in small time increments. The primary goal was to precisely compute the change in altitude, which is the key variable of interest in this simulation.

The altitude at any given time is determined by integration of velocity as a function of time, and velocity was obtained by integration of acceleration as a function of time. The value of acceleration depends on four primary variables: the rocket's mass, its weight, the thrust generated by the rocket motor and the aerodynamic drag.

The rocket's mass is solely influenced by the consumption of propellant, a process dictated by the propellant's properties, the geometry of the grain and the nozzle design. Once all the propellant is burned, the rocket's mass remains constant for the remainder of the simulation.

Weight is determined by the rocket's mass and the gravitational acceleration acting on it, which, as an approximation, depends solely on the rocket's altitude.

Thrust produced by the rocket motor is contingent upon the propellant's consumption rate, which in turn, is influenced by the properties of the propellant, the propellant grain geometry, the rocket motor nozzle design and the atmospheric pressure.

Aerodynamic drag is impacted by the rocket's geometry, particularly the surfaces in contact with the atmosphere. Additionally, whether the solid propellant is burning plays a role in drag. The drag from the rocket's tail is negligible while the propellant is burning but must be considered once it ceases to burn. The drag force also depends on the rocket's velocity and the properties of the surrounding fluid, specifically the Earth's atmosphere.

Throughout the simulation, atmospheric properties are modeled based on the rocket's altitude.

4. SOUNDING ROCKET

4.1. Selected Rocket

We have selected a rocket modeled around the Rexus-10 rocket from ESA, considering that it is a rocket that has experimental data that could be used to validate our model.

Figure 4.1. Photo from the Rexus-5 mission, which used the same rocket design as Rexus-10 (ESA, 2020).

Rexus, short for Rocket Experiments for University Students, is a sounding rocket mission included in the Rexus/Bexus program. The Rexus/Bexus program is a collaboration between the German Aerospace Center (DLR), the Swedish National Space Agency (SNSA), and the European Space Agency (ESA). Its primary objective is to provide university students with the opportunity to conduct scientific experiments in the near-space environment using sounding rockets and stratospheric balloons.

The Rexus-10, specifically, refers to the 10^{th} mission in the Rexus program.

This Rexus is a single stage rocket propelled by an Improved Orion solid propellant rocket motor that reaches an altitude of 82 km in this specific mission.

This rocket carried a payload of 112.3 kg and provided 180 seconds of reduced gravity flight.

Our goal is to use the experimental data about this rocket to confirm that our model can properly simulate the trajectory of flight of such rockets and be used to optimize some specific parameters of its design.

4.2. Rocket Technical Specifications

The technical specifications of our model are as close as we possibly to the ones of the Rexus-10, based on the information about this rocket available in (Schüttauf, 2017) and (REXUS 10, 2011).

Total length of the rocket: 5.60 m
Diameter of the rocket/rocket motor: 0.356 m
Length of rocket motor section: 2.80 m
Length of payload section: 1.38 m
Length of ogive section: 1.42 m
Number of fins: 3
Total area of each fin exposed to airflow: $A_{fin,w} = 0.643$ m^2
Ogive ratio: $4 \cdot d_{rm}$

Total mass of the rocket: 542 kg
Mass of propellant: 290 kg
Payload mass: 112.3 kg

4.3. Rocket Motor Technical Specifications

This rocket is composed of two hollow cylinders of different propellants, which we will be naming propellant 1 and propellant 2.

The propellant 1, the first to burn, is the inner cylinder. Propellant 2, the last one burning, is between propellant 1 and the outer shell of the rocket motor.

The hollow cylinder inside the rocket motor is 0.15 m in diameter.

The way that both propellants are structured inside the rocket motor chamber is showed in Figure 4.2.

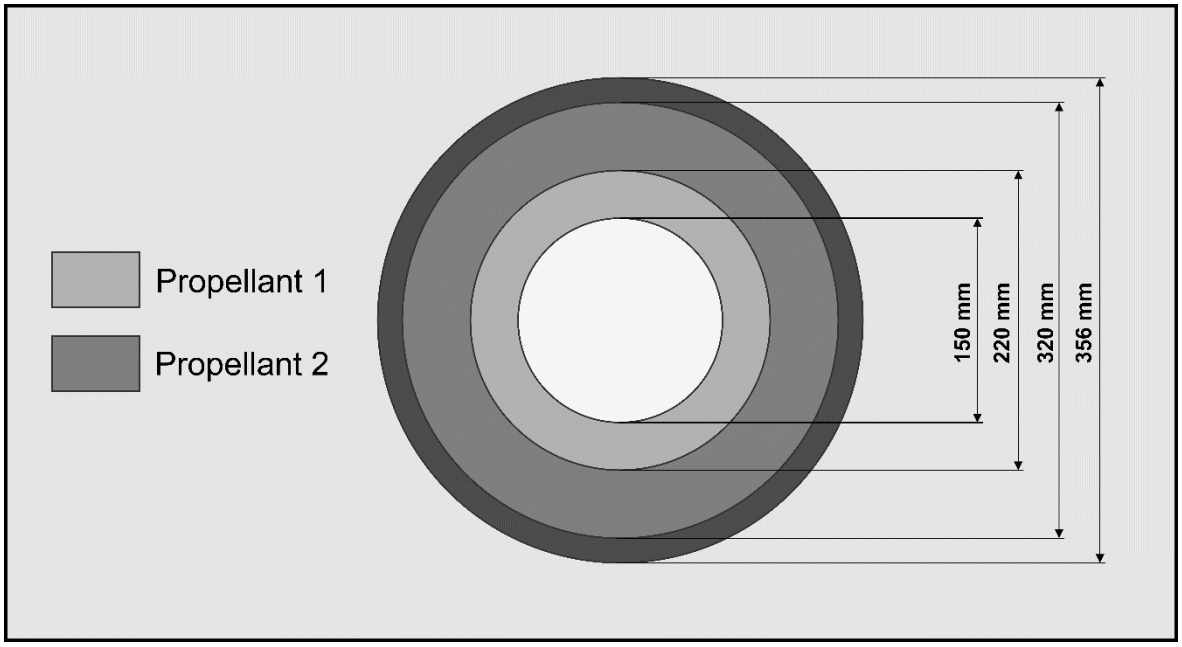

Figure 4.2. Diagram of the cross-section of the rocket motor chamber.

As stated in 2.3.1. the properties of the propellant's combustion products in the combustion chamber were obtained using NASA's CEA, while the composition of the propellant was picked according to experimental data available in the literature to obtain the desired flight behavior.

5. MODELING OF EARTH'S ATMOSPHERE

In the modeling of earth's atmosphere, we use different concepts of height, the geopotential height (*H*) and the geometric height (*Z*).

Since we are going to use the geometric height in the calculations of the distance travelled by the sounding rocket and the geopotential height to calculate some atmospheric properties, both will be used in different parts of the calculations.

The physical relation between these concepts follows Eq. 5.1 and Eq 5.2.

$$H = \frac{r_0 \cdot Z}{r_0 + Z} \tag{5.1}$$

$$Z = \frac{r_0 \cdot H}{r_0 - H} \tag{5.2}$$

5.1. Temperature

The calculations of atmospheric temperature were performed based on vast experimental data, according to (NOAA, NASA, & USAF, 1976), where it was divided the atmosphere into layers, based in their geopotential height, in which it is applied a linear temperature gradient, and is described in Eq. 5.3.

$$T_M = T_{M,b} + L_{M,b} \cdot (H - H_b) \tag{5.3}$$

The temperature returned by these equations returns a value for the molecular scale temperature, for which below 86 km of geometric altitude, there is no significant discrepancy from the value of kinetic temperature.

Table 5.1. Defined reference levels and gradients of the linearly segmented temperature-height profile from the surface to the geometric altitude of 86 km

Subscript b	**Molecular-scale Temperature** $T_{M,b}$ **(K)**	**Geopotential Height** H_b **(m')**	**Molecular-scale temperature gradient** $L_{M,b}$ **(K/m')**
0	288.15	0	-0.0065
1	216.65	11000	0.0
2	216.65	20000	+0.001
3	228.65	32000	+0.0028
4	270.65	47000	0.0
5	270.65	51000	-0.0028
6	214.65	71000	-0.002
7	186.67	84852	

So, based on Table 5.1, we get the equations from Eq 5.4 to Eq 5.10, to calculate the temperature for each layer of the atmosphere until the geopotential height of 84852 m, depending on the altitude range.

From 0 m to 11000 m:

$$T_M = 288.15 - 0.0065 \cdot (H) \tag{5.4}$$

From 11000 m to 20000 m:

$$T_M = 216.65 \tag{5.5}$$

From 20000 m to 32000 m:

$$T_M = 216.65 + 0.001 \cdot (H - 20000) \tag{5.6}$$

From 32000 m to 47000 m:

$$T_M = 228.65 + 0.0028 \cdot (H - 32000) \quad 5.7$$

From 47000 m to 51000 m:

$$T_M = 270.65 \quad 5.8$$

From 51000 m to 71000 m:

$$T_M = 270.65 - 0.0028 \cdot (H - 51000) \quad 5.9$$

From 71000 m to 84852 m:

$$T_M = 214.65 - 0.002 \cdot (H - 71000) \quad 5.10$$

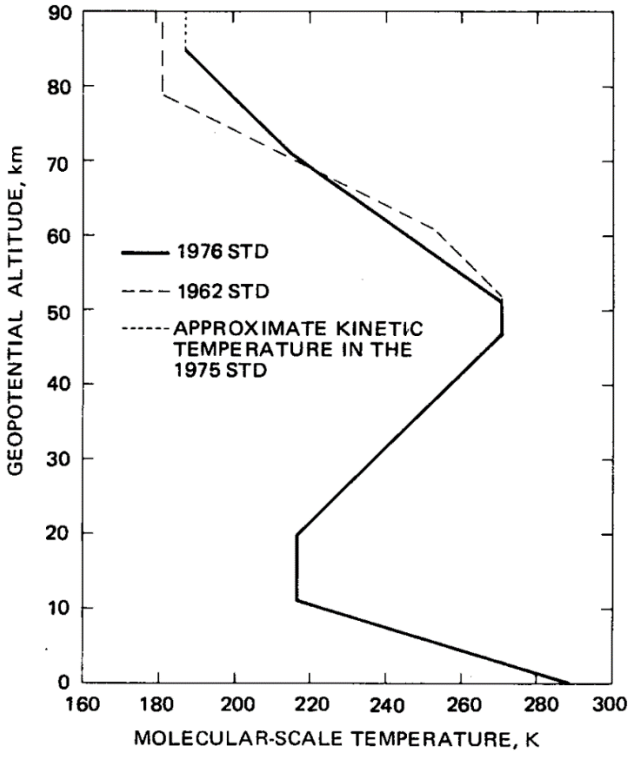

Figure 5.1. Molecular-scale temperature as a function of geopotential altitude **(NOAA, NASA, & USAF, 1976)**.

For the case where geometric altitude is above 86 km, values of T_M are no longer defined, and geopotential is no longer the primary argument. Here, the temperature altitude profile is defined in terms of four successive functions, in which the first derivative of T with respect to Z is continuous over the entire altitude region, 86 km to 1000 km.

The layer from 86 km to 91 km is isothermal, the layer from 91 to 110 km has the form of an ellipse, the layer from 110 to 120 km is a positive gradient layer, and the layer from 120 to 1000 km increases exponentially towards an asymptote, where the temperature is 1000 K.

In Table 5.2 are presented the kinetic temperature at some given geometric altitudes and kinetic temperature gradient at some given altitude ranges, or in some ranges, the shape of the function.

Table 5.2. Defined reference levels and gradients of the segmented temperature-height profile from 86 km to 1000 km

Subscript b	**Kinetic Temperature** T_b **(K)**	**Geometric Height** Z_b **(m)**	**Kinetic-temperature gradient** $L_{k,b}$ **(K/m)**
7	186.87	86000	0.0
8	186.87	91000	(elliptical)
9	240	110000	+0.012
10	360	120000	(exponential)
11	270.65	500000	(exponential)
12	1000	1000000	(exponential)

With this data, the equations of temperature for each given layer can be described by Eq. 5.11, Eq. 5.13, Eq. 5.15 and Eq. 5.17.

From 86000 m to 91000 m the temperature remains constant:

$$T_k = 186.87 \tag{5.11}$$

From 91000 m to 110000 m:

$$T_k = T_e + A \cdot \sqrt{1 - \left(\frac{Z - Z_8}{a_e}\right)^2} \quad 5.12$$

$T_e = 263.1905$ K, $A = -76.3232$ K, and $a_e = -19942.9$ m, so:

$$T_k = 263.1905 - 76.3232 \cdot \sqrt{1 - \left(\frac{Z - 91000}{-19942.9}\right)^2} \quad 5.13$$

From 110000 m to 120000 m:

$$T_k = T_9 + L_{K,9} \cdot (Z - Z_9) \quad 5.14$$

$$(=)$$

$$T_k = 240 + 0.012 \cdot (H - 110000) \quad 5.15$$

From 120000 m to 1000000 m:

$$T_k = T_\infty - (T_\infty - T_{10}) \cdot e^{-\lambda \cdot \xi} \quad 5.16$$

Where:

$\lambda = \frac{L_{K,9}}{T_\infty - T_{10}} = 0.0001875$ and

$\xi = \xi(Z) = \frac{(Z - Z_{10}) \cdot (r_0 + Z_{10})}{(r_0 + Z)}$

$$T_k = 1000 - (1000 - 360) \cdot e^{-0.0001875 \cdot \left(\frac{(Z - 120000) \cdot (r_0 + 120000)}{(r_0 + Z)}\right)} \quad 5.17$$

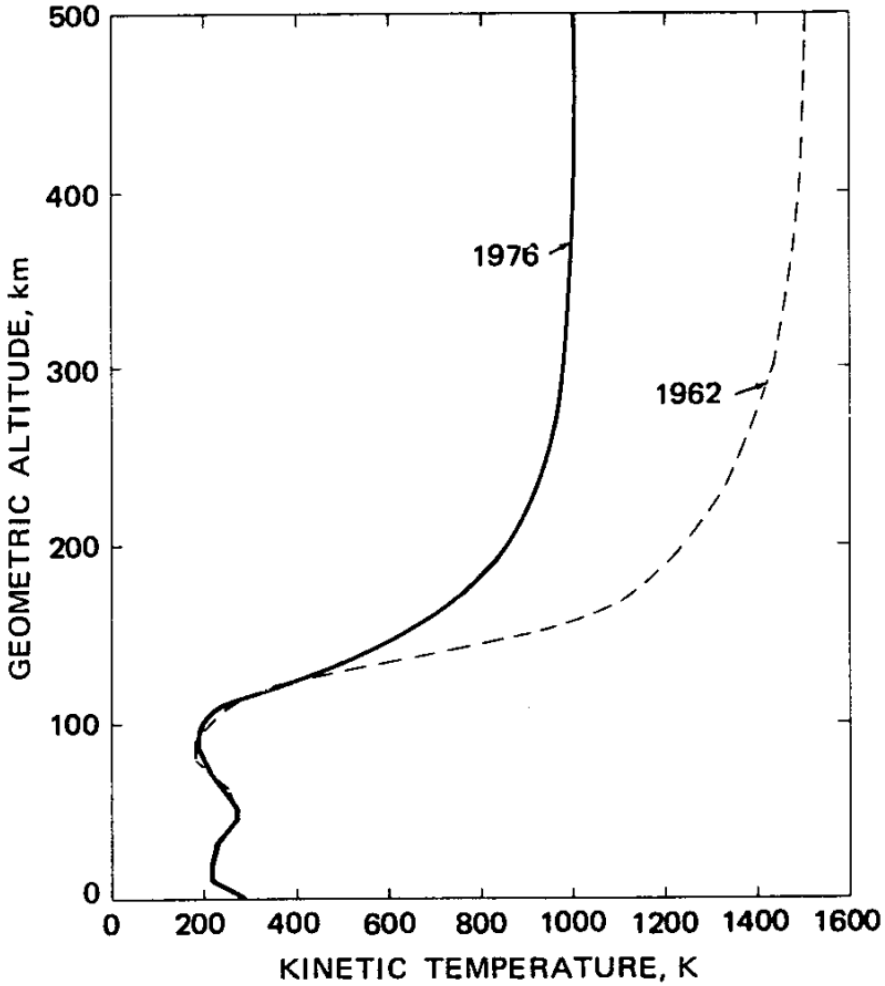

Figure 5.2. Kinetic temperature as a function of geometric altitude **(NOAA, NASA, & USAF, 1976)**.

5.2. Pressure

For pressure, according to (NOAA, NASA, & USAF, 1976), until 86 km of geometric altitude, it can be modeled in the same layers as the temperature.

The pressure value is given by two equations, one for when $L_{M,b}$ for a particular layer is not equal to zero, in Eq. 5.18.

$$P = P_b \cdot \left[\frac{T_{M,b}}{T_{M,b} + L_{M,b} \cdot (H - H_b)}\right]^{\left[-\frac{g\prime_0 \cdot M_0}{R^* \cdot L_{M,b}}\right]} \quad 5.18$$

And Eq. 5.19 for when the value of $L_{M,b}$ is equal to zero.

$$P = P_b \cdot e^{\left[-\frac{g\prime_0 \cdot M_0 \cdot (H - H_b)}{R^* \cdot T_{M,b}}\right]} \quad 5.19$$

With the help of Table 5.1, we can create the equations that gives us the pressure values for each layer, considering its geopotential altitude as such, given by Eq. 5.20 to Eq 5.26.

From 0 m to 11000 m:

$$P = 101325 \cdot \left[\frac{288.15}{288.15 - 0.0065 \cdot (H)}\right]^{\left[-\frac{9.80665 \cdot 0.0289644}{8.31432 \cdot (-0.0065)}\right]} \quad 5.20$$

From 11000 m to 20000 m:

$$P = 22632.1 \cdot e^{\left[-\frac{9.80665 \cdot 0.0289644 \cdot (H - 11000)}{8.31432 \cdot 216.65}\right]} \quad 5.21$$

From 20000 m to 32000 m:

$$P = 5474.87 \cdot \left[\frac{216.65}{216.65 + 0.001 \cdot (H - 20000)}\right]^{\left[-\frac{9.80665 \cdot 0.0289644}{8.31432 \cdot 0.001}\right]} \quad 5.22$$

From 32000 m to 47000 m:

$$P = 868.016 \cdot \left[\frac{228.65}{228.65 + 0.0028 \cdot (H - 32000)}\right]^{\left[-\frac{9.80665 \cdot 0.0289644}{8.31432 \cdot 0.0028}\right]} \quad 5.23$$

From 47000 m to 51000 m:

$$P = 110.906 \cdot e^{\left[-\frac{9.80665 \cdot 0.0289644 \cdot (H - 47000)}{8.31432 \cdot 270.65}\right]} \quad 5.24$$

From 51000 m to 71000 m:

$$P = 66.9387 \cdot \left[\frac{270.65}{270.65 - 0.0028 \cdot (H - 51000)}\right]^{\left[-\frac{9.80665 \cdot 0.0289644}{8.31432 \cdot (-0.0028)}\right]} \quad 5.25$$

From 71000 m to 84852 m:

$$P = 3.95641 \cdot \left[\frac{214.65}{214.65 - 0.002 \cdot (H - 71000)}\right]^{\left[-\frac{9.80665 \cdot 0.0289644}{8.31432 \cdot (-0.002)}\right]} \quad 5.26$$

From 84852 m of geopotential altitude or 86000 m or geometric altitude, it was introduced a method of calculation that we used in our program multiple times, the Lagrange polynomial (Polynomial interpolation, 2023), based on an available set of data.

Since the formula used to calculate the pressure beyond 86000 m uses very complicated calculations, we decided to take a different approach and use the experimental

data provided in (NOAA, NASA, & USAF, 1976), where there is a table of values of pressure correspondent to a vast amount of geometric altitude values.

It was written a section of code in which, for the altitude that a given correspondent pressure was required, and comparing it to the set of data available, it was used the data of the 3 altitudes with data available below the altitude of interest, and 3 altitudes above, so that if the program asked to know the pressure at an altitude of, for example, 173327 m, the code would inspect the data available and use the values of pressure in the data available for 172000, 172500, 173000, 173500, 174000 and 174500 meters of altitude and, with those 6 nodes, create a Lagrange interpolating polynomial that would be used to calculate the value of pressure for the altitude of 173327 m.

It was found via numerical analysis on Excel that this method returned a relative error of less than 0.008% for the whole range of altitude, from 120 km to 1000 km.

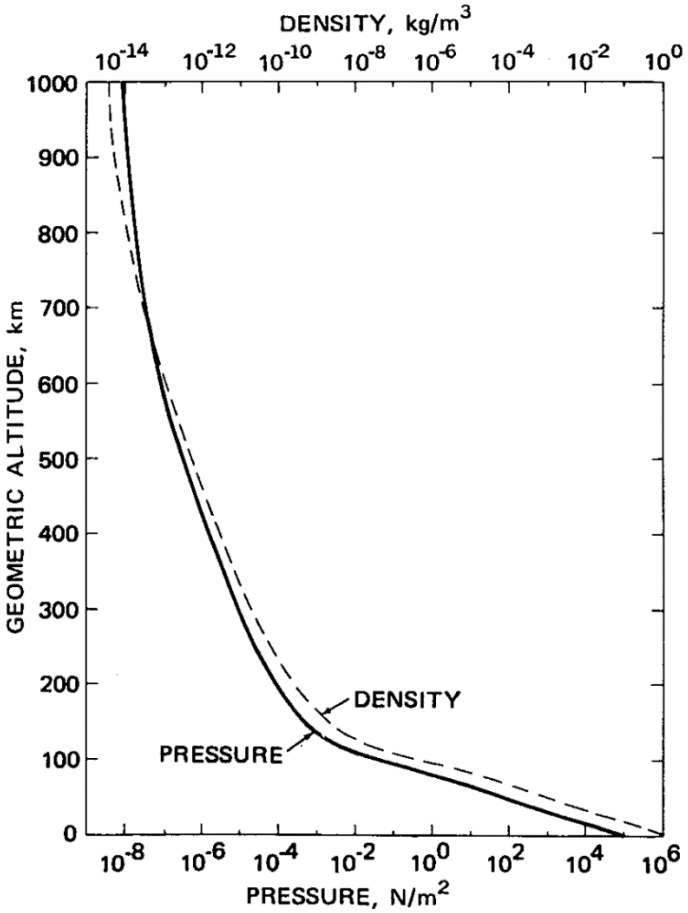

Figure 5.3. Pressure as a function of geometric altitude **(NOAA, NASA, & USAF, 1976)**.

5.3. Molar Mass

The molar mass remains constant in the range of altitude between 0 km and 86 km, at a value of $M_{air} = 0.0289644$ kg/mol.

In the range from 86 km to 1000 km, it was also used here the Lagrange interpolating polynomial, based on the table from (NOAA, NASA, & USAF, 1976), in which are given values of M_{air} correspondent to a vast number of altitude values.

It was found via numerical analysis on Excel that this method returned a relative error of less than 0.2% for the whole range of altitude, from 120 km to 1000 km.

This relative error is still significantly smaller than the inherent error introduced by atmospheric variations or by the sensors used to record such experimental data.

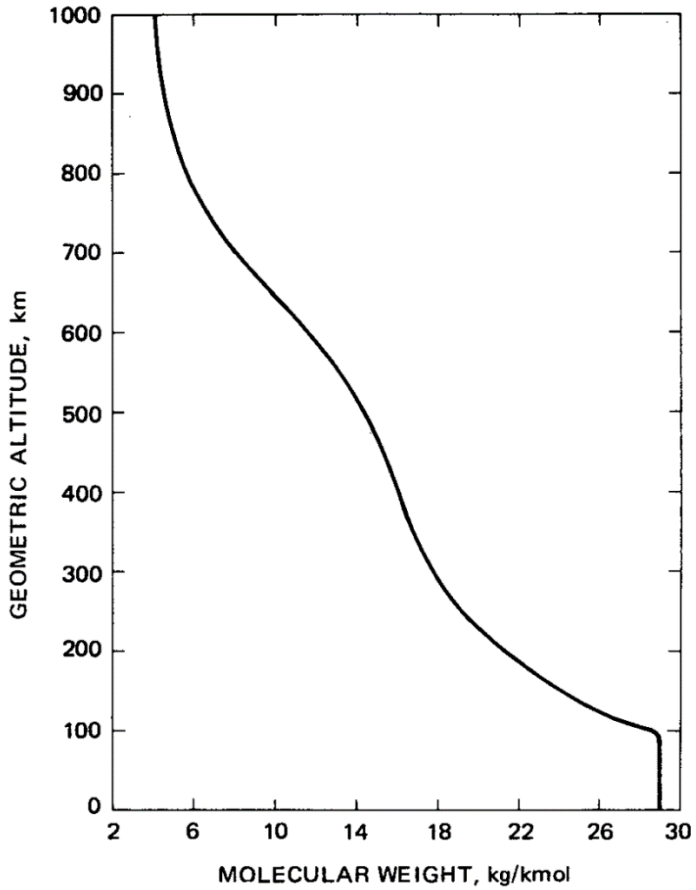

Figure 5.4. Molecular weight as a function of geometric altitude **(NOAA, NASA, & USAF, 1976)**.

5.4. Density

Although less accurate at higher altitudes, the Ideal Gas Law can still be applied to obtain a good approximation of the density of air at high altitudes using Eq 5.27, from NOAA (NOAA, NASA, & USAF, 1976).

$$\rho_{air} = \frac{P \cdot M_{air}}{R^* \cdot T_k} \qquad 5.27$$

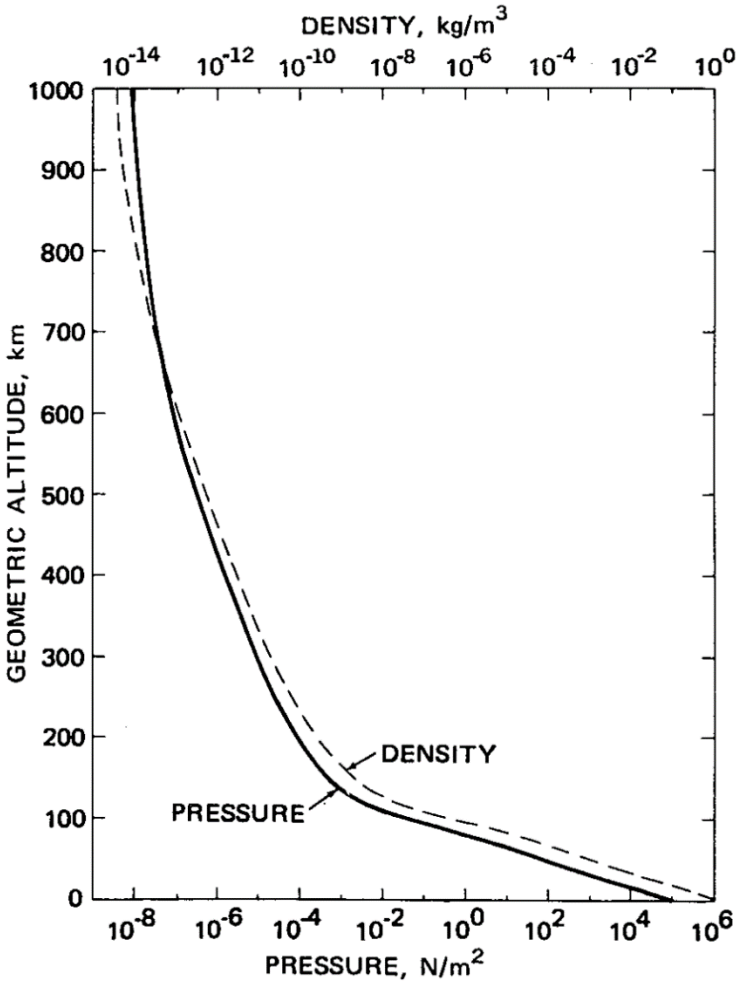

Figure 5.5. Density as a function of geometric altitude **(NOAA, NASA, & USAF, 1976)**.

5.5. Specific Heat Ratio

The specific heat ratio remains constant, at a value of 1.4, up to an altitude of 86 km.

From 86 km to 1000 km of altitude, as the composition of earth's atmosphere changes significantly, its specific heat ratio will also suffer changes.

The atmosphere composition is given in NOAA (NOAA, NASA, & USAF, 1976), where it is provided a table with the number density of the six main species, N_2, O, O_2, Ar, He and H, present on the earth's atmosphere from 86 km to 1000 km, correspondent to a vast number of altitude values.

In order to accurately obtain the number density of each of those species for the whole continuous altitude range, a method using the Lagrange interpolating polynomial, as previously described, was used.

The molar fraction of each species *i* in the atmosphere x_i is calculated using Eq. 5.28 where n_i is the number density of species *i*.

$$x_i = \frac{n_i}{\sum_{i=1}^{6} n_i} \tag{5.28}$$

To calculate the specific heat at constant pressure relative to each species *i*, was used Eq. 5.29, from NASA RP-1311 (Gordon & McBride, 1994).

$$C_{p,i} = R^* \cdot \left(a_1 \cdot {T_k}^{-2} + a_2 \cdot {T_k}^{-1} + a_3 + a_4 \cdot T_k + a_5 \cdot {T_k}^2 + a_6 \cdot {T_k}^3 + a_7 \cdot {T_k}^4\right) \tag{5.29}$$

Where the constants a_1 to a_7 are obtained from NASA Thermo Build (Snyder, 2020), for each species *i* in the temperature range 200 K to 1000 K.

Now we can calculate atmosphere *Cp* using Eq. 5.30.

$$C_p = x_{N_2} \cdot C_{p,N_2} + x_O \cdot C_{p,O} + x_{O_2} \cdot C_{p,O_2} + x_{Ar} \cdot C_{p,Ar} + x_{He} \cdot C_{p,He} + x_H \cdot C_{p,H} \tag{5.30}$$

The specific heat ratio can be characterized by Eq. 5.31, from NOAA (NOAA, NASA, & USAF, 1976).

$$\gamma_{air} = \frac{C_p}{C_v} \quad (=) \quad \gamma_{air} = \frac{C_p}{C_p - R^*} \tag{5.31}$$

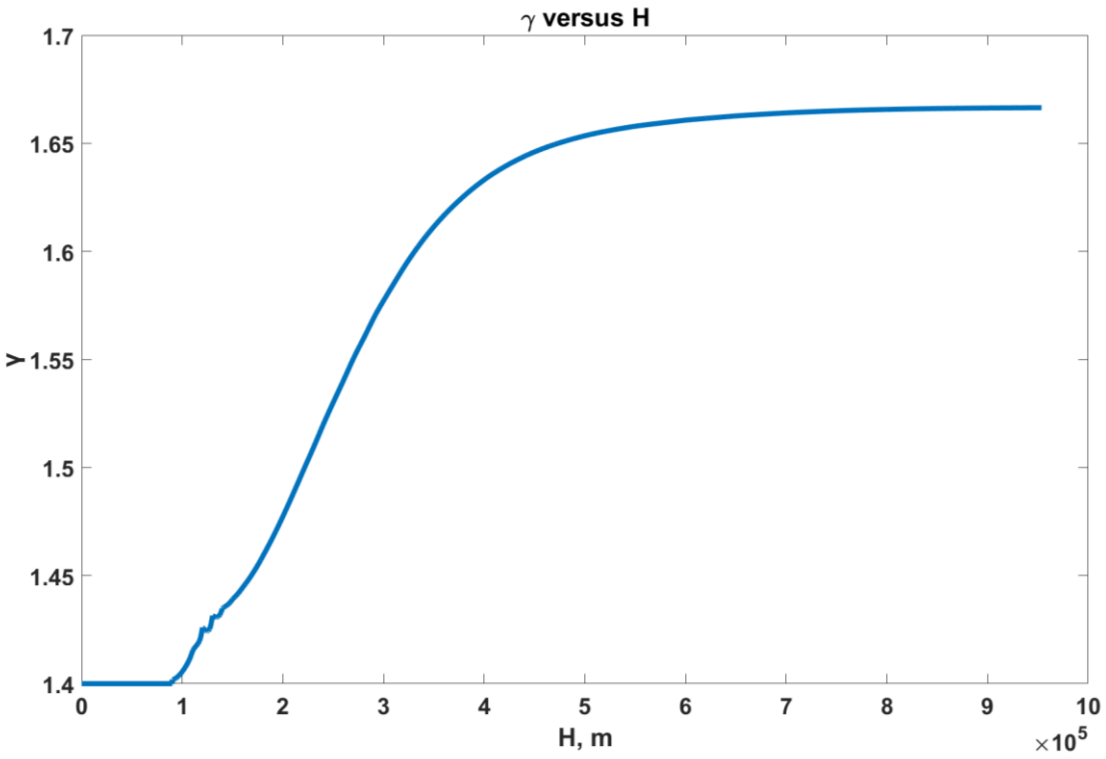

Figure 5.6. Specific heat ratio as a function of geometric altitude.

5.6. Speed of Sound

Speed of sound is calculated by Eq 5.32, from NOAA (NOAA, NASA, & USAF, 1976).

$$C_s = \sqrt{\frac{\gamma_{air} \cdot R^* \cdot T_k}{M_{air}}} \qquad 5.32$$

According to NOAA (NOAA, NASA, & USAF, 1976), this equation applies only when the sound wave is a small perturbation on the ambient condition.

The limitations of the concept of speed of sound due to extreme attenuation are also of concern.

For this reason, the concept of speed of sound progressively loses its range of applicability at high altitudes, above 86 km.

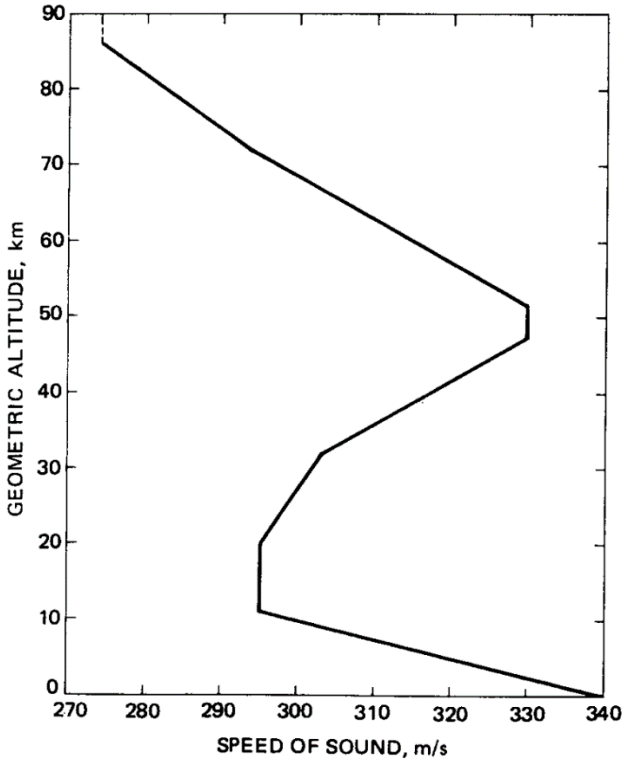

Figure 5.7. Speed of sound as a function of geometric altitude **(NOAA, NASA, & USAF, 1976)**.

5.7. Dynamic Viscosity

The equation to calculate the dynamic viscosity μ, according to NOAA (NOAA, NASA, & USAF, 1976), is derived from kinetic theory, containing constants obtained based in experimentation, is expressed in Eq. 5.33, from NOAA (NOAA, NASA, & USAF, 1976).

$$\mu = \frac{\beta \cdot T^{3/2}}{T_k + S} \tag{5.33}$$

in which $\beta = 1.458 \cdot 10^{-6}$ kg/(s·m·K$^{1/2}$) and $S = 110.4$ K.

This equation is not usable in very high or very low temperatures, or at great altitudes. For this reason, it's only considered a good approximation until 86 km of altitude.

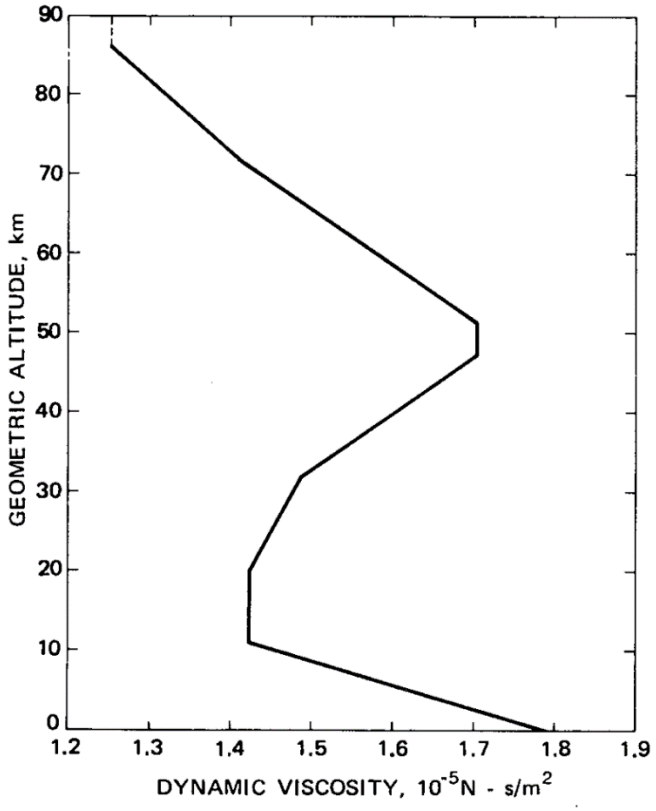

Figure 5.8. Dynamic viscosity as a function of geometric altitude **(NOAA, NASA, & USAF, 1976)**.

6. ROCKET MOTION MODEL

6.1. Forces Acting on The Rocket

The forces acting in the rocket are the rocket weight, the aerodynamic drag and the rocket motor thrust.

All forces act in the vertical orientation. The rocket weight and the aerodynamic direction are opposed to the direction of the motion of the rocket, while thrust has the same direction as the motion of the rocket.

The vectorial sum of these forces is equal to the product of the rocket mass times its acceleration, resulting in Eq. 6.13, that is used to calculate acceleration at any given time instant.

$$\vec{W} + \vec{D} + \vec{T} = m\,\vec{a} \tag{6.1}$$

$$W + D + T = ma \tag{6.2}$$

$$a = \frac{W + D + T}{m} \tag{6.3}$$

6.2. Motion Equations

The equations of motion, related to the variable time, t , can be derived as such:

$$a = \frac{dv}{dt} \tag{6.4}$$

$$dv = a\,dt \tag{6.5}$$

$$\int_{v_0}^{v} dv = \int_{t_0}^{t} a\,dt \tag{6.6}$$

$$[v]_{v_0}^{v} = a \cdot [t]_{t_0}^{t} \tag{6.7}$$

$$v - v_0 = a \cdot (t - t_0) \tag{6.8}$$

Where Eq. 6.9 returns the value for the variable velocity at any instant.

$$v = v_0 + a \cdot (t - t_0) \tag{6.9}$$

$$v = \frac{dZ}{dt} \tag{6.10}$$

$$\frac{dZ}{dt} = v_0 + a \cdot (t - t_0) \tag{6.11}$$

$$\frac{dZ}{dt} = v_0 + a \cdot t - a \cdot t_0 \tag{6.12}$$

$$dZ = v_0 \cdot dt - a \cdot t_0 \cdot dt + a \cdot t \cdot dt \tag{6.13}$$

$$\int_{Z_0}^{Z} dZ = \int_{t_0}^{t} v_0 \cdot dt - \int_{t_0}^{t} a \cdot t_0 \cdot dt + \int_{t_0}^{t} a \cdot t \cdot dt \quad 6.14$$

$$[Z]_{Z_0}^{Z} = v_0[t]_{t_0}^{t} - at_0[t]_{t_0}^{t} + a\left[\frac{t^2}{2}\right]_{t_0}^{t} \quad 6.15$$

$$Z - Z_0 = v_0(t - t_0) - at_0(t - t_0) + \frac{1}{2}a(t^2 - t_0^2) \quad 6.16$$

Which comes down to the equation that gives us the position of the rocket at any point in time, expressed in Eq.6.17.

$$Z = Z_0 + v_0(t - t_0) - at_0(t - t_0) + \frac{1}{2}a(t^2 - t_0^2) \quad 6.17$$

6.3. Weight Model

The weight force acting upon the rocket has vertical orientation, its direction is pointing to the surface, and is only dependent on the variables mass and gravity acceleration, as defined in Eq. 6.18.

$$W = -mg \tag{6.18}$$

Gravity acceleration was already defined in 2.5, and is dependent on the altitude of the rocket, according to Eq. 6.19.

$$g = 9.80655 \cdot \frac{{r_0}^2}{(r_0 + Z)^2} \tag{6.19}$$

In the constraints of our model, the rocket's mass is only affected by the burn of the propellant, that burns in a cylindrical surface inside the rocket motor, with a variable burning rate, which is governed by Eq. 6.20.

$$\frac{dm}{dt} = \frac{\rho_b \cdot l_b \cdot \pi \cdot \frac{\left(d_b + 2 \cdot dt \cdot r_p\right)^2 - {d_b}^2}{4}}{dt} \tag{6.20}$$

Where r_p is obtained from Eq. 6.21, according to Vieille's Law, from Combustion and Flame (S. Isert, L. Xin, J. Xie, & S.F. Son, 2017).

$$r_p = a_p \cdot 10^{-3} \cdot \left(\frac{P_c}{10^6}\right)^{n_p} \tag{6.21}$$

The variable P_c can be calculated using Eq. 6.22, from Sutton (Biblarz & P. Sutton, 2017).

$$P_c = \left[\frac{(10^6)^{n_p}}{10^{-3}} \cdot \frac{1}{a_p \cdot \rho_p \cdot A_b} \cdot \frac{C_e \cdot A_t}{\sqrt{\frac{R^* \cdot T_b}{M_b}}} \cdot \sqrt{\gamma_p} \cdot \left(\frac{2}{\gamma_p + 1} \right)^{\frac{\gamma_p + 1}{2 \cdot (\gamma_p - 1)}} \right]^{\frac{1}{n_p - 1}} \quad 6.22$$

Where A_b is the propellant burning area and can be obtained from Eq. 6.23.

$$A_b = d_b \cdot \pi \cdot l_b \quad 6.23$$

This way, having a burning rate of the propellant in a given time interval dt, and knowing the initial mass of propellant left, the mass at the end of that time interval can be calculated through Eq. 6.24.

$$m_{p,f} = m_{p,i} - \frac{dm}{dt} \cdot dt \quad 6.24$$

Knowing this, we can find the total mass of the rocket at any instant in time, as expressed in Eq. 6.25.

$$m = m_{er} + m_{payload} + m_p \quad 6.25$$

After burning the whole mass of the propellant, in our model, the total mass of the rocket will become a constant that represents the sum of the mass of the empty rocket with the mass of the payload.

6.4. Thrust Model

The thrust given by the rocket motor is, according to Sutton (Biblarz & P. Sutton, 2017), defined by Eq. 6.26.

$$T = \dot{m} \cdot v_e + (P_e - P_{air}) \cdot A_e \tag{6.26}$$

We can find the value of P_e solving Eq. 6.27, from Sutton (Biblarz & P. Sutton, 2017).

$$\frac{A_t}{A_e} = \left(\frac{\gamma_p + 1}{2}\right)^{\frac{1}{\gamma_p - 1}} \cdot \left(\frac{P_e}{P_c}\right)^{\frac{1}{\gamma_p}} \cdot \sqrt{\frac{\gamma_p + 1}{\gamma_p - 1} \cdot \left[1 - \left(\frac{P_e}{P_c}\right)^{\frac{\gamma_p - 1}{\gamma_p}}\right]} \tag{6.27}$$

Since we cannot solve the equation in order of variable of P_e, we will have to equal it to zero, as in Eq. 6.28, to be able to solve it using an iterative method.

$$\frac{A_t}{A_e} - \left(\frac{\gamma_p + 1}{2}\right)^{\frac{1}{\gamma_p - 1}} \cdot \left(\frac{P_e}{P_c}\right)^{\frac{1}{\gamma_p}} \cdot \sqrt{\frac{\gamma_p + 1}{\gamma_p - 1} \cdot \left[1 - \left(\frac{P_e}{P_c}\right)^{\frac{\gamma_p - 1}{\gamma_p}}\right]} = 0 \tag{6.28}$$

This way, we can use the Newton-Raphson (Newton's method, 2023) method to find out for which value of P_e Eq. 6.28 becomes true, which is the value we are looking for.

Finally, the value of the flow velocity at the exit section of the nozzle, or exhaust, can be obtained using Eq. 6.29, from Sutton (Biblarz & P. Sutton, 2017).

$$v_e = \sqrt{\frac{2 \cdot \gamma_p}{\gamma_p - 1}} \cdot \frac{R^* \cdot T_b}{M_b} \cdot \left(\frac{P_e}{P_c}\right)^{\frac{\gamma_p - 1}{\gamma_p}} \tag{6.29}$$

6.5. Aerodynamic Drag Model

In the aerodynamic drag model, since velocity is squared, it will always return a positive value for drag, regardless of the direction of the rocket's motion.

Because of this and considering that drag is a force applied in the direction opposite of the direction of the motion, the simulation will have to use two different formulas, one for the instants where velocity has a positive value, and other for the instants where velocity has a negative value according to Eq 6.30 or Eq 6.31, from White (White, 2017).

$$D = -C_x \cdot A_f \cdot \frac{1}{2} \cdot \rho \cdot v^2 \tag{6.30}$$

$$D = C_x \cdot A_f \cdot \frac{1}{2} \cdot \rho \cdot v^2 \tag{6.31}$$

For the calculations of drag, we separated the rocket into three relevant segments, the ogive, the fins, and the rocket fuselage, that contains all the cylindrical area of the rocket in contact with the fluid.

When the rocket motor stops burning, we must consider the drag related to the tail of the rocket as well.

Since we are using experimental data to calculate the drag of the ogive, in the three components we will calculate the value based on Eq 6.32 or Eq 6.33.

$$D = (C_x \cdot A)_{total} \cdot \frac{1}{2} \cdot \rho \cdot v^2 \tag{6.32}$$

$$D = -(C_x \cdot A)_{total} \cdot \frac{1}{2} \cdot \rho \cdot v^2 \tag{6.33}$$

Where:

$$(C_x \cdot A)_{total} = (C_x \cdot A)_{ogive} + (C_x \cdot A)_{fin} + (C_x \cdot A)_{fus} + (C_x \cdot A)_{tail} \tag{6.34}$$

According to White (White, 2017), the calculations of $(C_x \cdot A)$ for the fins and fuselage will use different equations when the value of Re is below $5 \cdot 10^5$ and when the value of Re is above $5 \cdot 10^5$.

In the ogive, $(C_x \cdot A)_{ogive}$, is given as a set of three equations for three different flow regions. A region of subsonic flow for values of Ma below 0.7, a region of transonic flow for values of Ma from 0.7 to 1.2, and a region of supersonic flow for values of values of Ma above 1.2.

The value of Re for the fins segment is given by Eq. 6.35, from White (White, 2017).

$$Re_{fin} = \frac{c_{fin,m} \cdot |v| \cdot \rho_{air}}{\mu_{air}} \quad 6.35$$

The value of Re for the fuselage segment is given by Eq. 6.36.

$$Re_{fus} = \frac{l_{fus} \cdot |v| \cdot \rho_{air}}{\mu_{air}} \quad 6.36$$

Where $c_{fin,m} = 0.574$ m and $l_{fus} = 4.18$ m.

6.5.1. Fuselage Drag

Coefficient of drag for the fuselage when $Re_{fus} < 5 \cdot 10^5$ is given by Eq. 6.37, from White (White, 2017).

$$C_{x_{fus}} = \frac{0.664}{\sqrt{Re_{fus}}} \quad 6.37$$

Coefficient of drag for the fuselage when $Re_{fus} \geq 5 \cdot 10^5$ is given by Eq. 6.38, from White (White, 2017).

$$C_{x_{fus}} = \frac{0.0155}{Re_{fus}{}^{1/7}} - \frac{720}{Re_{fus}} \tag{6.38}$$

Therefore:

$$(C_x \cdot A)_{fus} = C_{x_{fus}} \cdot A_{fus,w} \tag{6.39}$$

6.5.2. Fin Drag

Coefficient of drag for the fins when $Re_{fin} < 5 \cdot 10^5$ is given by Eq 6.40.

$$C_{x_{fin}} = \frac{0.664}{\sqrt{Re_{fin}}} \tag{6.40}$$

Coefficient of drag for the fuselage when $Re_{fin} \geq 5 \cdot 10^5$ is given by Eq 6.41.

$$C_{x_{fin}} = \frac{0.0155}{Re_{fin}{}^{1/7}} - \frac{720}{Re_{fin}} \tag{6.41}$$

Therefore, we have Eq. 6.42.

$$(C_x \cdot A)_{fin} = C_{x_{fin}} \cdot A_{fin,w} \tag{6.42}$$

6.5.3. Ogive Drag

For the ogive, based on (Hoerner, 1965), we found 3 different formulas for each region of flow.

6.5.3.1. Subsonic Drag

For subsonic drag, the component of drag coefficient multiplied by surface area, relative to the ogive, is given by Eq. 6.43.

$$(C_x \cdot A)_{ogive} = 0.75 * 0.37 * A_{ogive} \quad 6.43$$

6.5.3.2. Transonic Drag

For transonic drag, the component of drag coefficient multiplied by surface area, relative to the ogive, is given by Eq. 6.44.

$$(C_x \cdot A)_{ogive} = 0.75 \cdot (-1.3978 \cdot |Ma|^3 + 3.8756 \cdot |Ma|^2 - 3.4109 \cdot |Ma| + 1.3383) \cdot A_{ogive} \quad 6.44$$

6.5.3.3. Supersonic Drag

For supersonic drag, the component of drag coefficient multiplied by surface area, relative to the ogive, is given by Eq. 6.45.

$$(C_x \cdot A)_{ogive} = 0.75 \cdot (1.7771 \cdot 10^{-4} \cdot |Ma|^6 - 5.1863 \cdot 10^{-3} \cdot |Ma|^5 + 6.0622 \cdot 10^{-2} \cdot |Ma|^4 - 3.6226 \cdot 10^{-1} \cdot |Ma|^3 + 1.1672 \cdot |Ma|^2 - 1.9417 \cdot |Ma| + 1.5624) \cdot A_{ogive} \quad 6.45$$

6.5.4. Tail Drag

For when there is no combustion, the drag from the tail of the rocket must be taken into consideration, according to Eq. 6.46.

$$(C_x \cdot A)_{tail} = 0.7 \cdot A_{tail} \quad 6.46$$

7. EXPERIMENTAL RESULTS OBTAINED FROM THE REXUS-10 MISSION

Here, we present some of the experimental results obtained from the Rexus-10 mission, which are available in the literature. These results will be used to compare and validate the model created for the simulations.

General information

Launch site Esrange Space Center
Launch date February 23, 2011, at 10:00 UTC
Customer Student programme

Technical information

Rocket type	Improved Orion rocket
Nominal diameter	356 mm
Total weight	542 kg
Burning time 1st stage	26 s
Max acceleration	21 g
Apogee	~82 km
Flight time to apogee	~144 s

Experiment modules

DLR sponsored experiments:
– GAGa (Otto-von-Guericke University Magdeburg, Germany): Granular Anisotropic Gases – a study of the effects of anisotropy on granular gas dynamics.
– FOCUS (Technical University of Munich, Germany): First Orbit Curing Experiment of University Students – development and flight testing of a deployable structure with a resin matrix that will be cured after deployment.
ESA/SNSB sponsored experiments:
– SQUID (KTH Royal Institute of Technology in Stockholm, Sweden): Spinning QUad Ionospheric Deployer – wire-boom deployment system.
– M-BEAM (Higher Technical College of Electronics, Moessingerstrasse, Austria): Magnetic BEAring for brushless DC Motor – determining of magnetic bearings for an asynchronous motor for maintenance-free operation of the gyroscope in microgravity.

Figure 7.1. Details from the Rexus-10 mission **(REXUS 10, 2011)**.

Graphical information correlating altitude with respect to time for the Rexus rocket in multiple missions was also available. This information includes data on parachute deployment, which was not considered in the model implemented by our simulations.

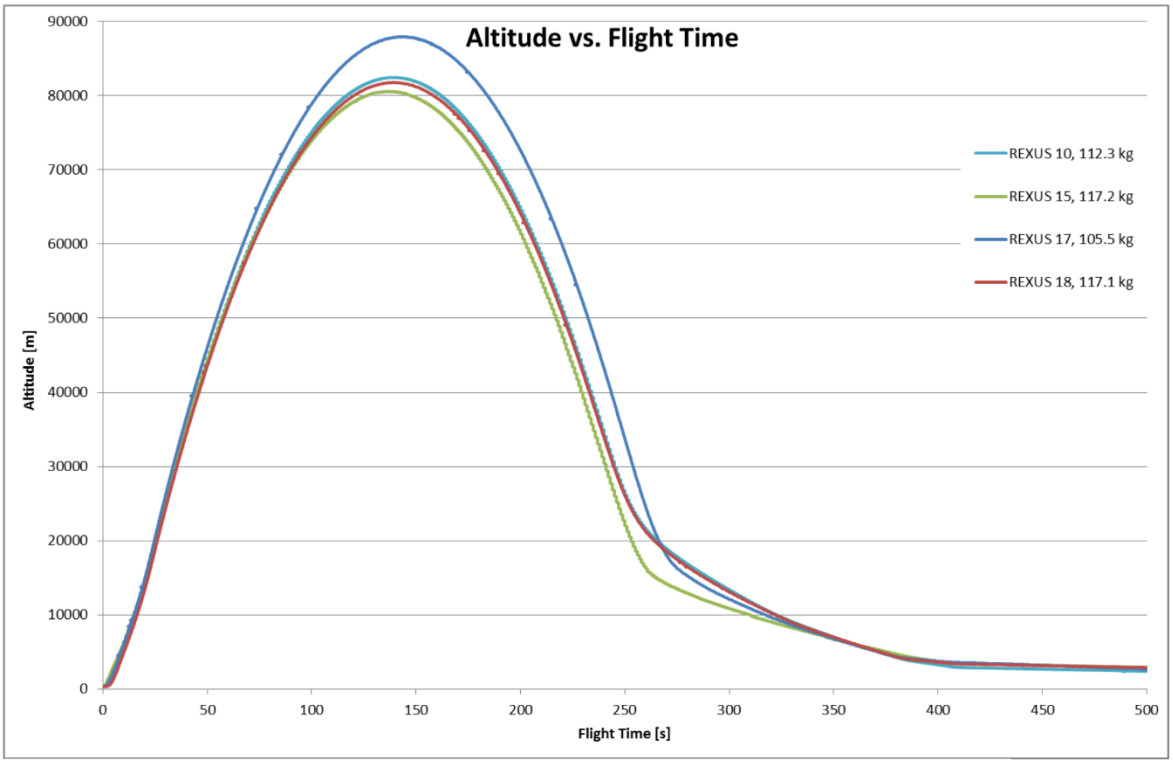

Figure 7.2. Altitude as a function of time **(Schüttauf, 2017)**.

8. RESULTS AND ANALYSIS OF THE SIMULATIONS

In this chapter, the objective is to study the effects of the nozzle's throat diameter in flight performance.

It will also be studied the effects of the mass of payload in flight performance.

For this, graphs based on data from a set of simulations will be performed in the program.

8.1. Effect of Nozzle Throat Diameter in Flight Performance

To gauge the effect of nozzle's throat diameter in flight performing, the maximum altitude of the rocket will be analyzed.

Simulations will be made where the payload of the rocket is fixed at 112.3 kg, in which the nozzle's throat diameter will be the only variable that changes its value, from 0.09 m to 0.14 m in increments of 0.002 m.

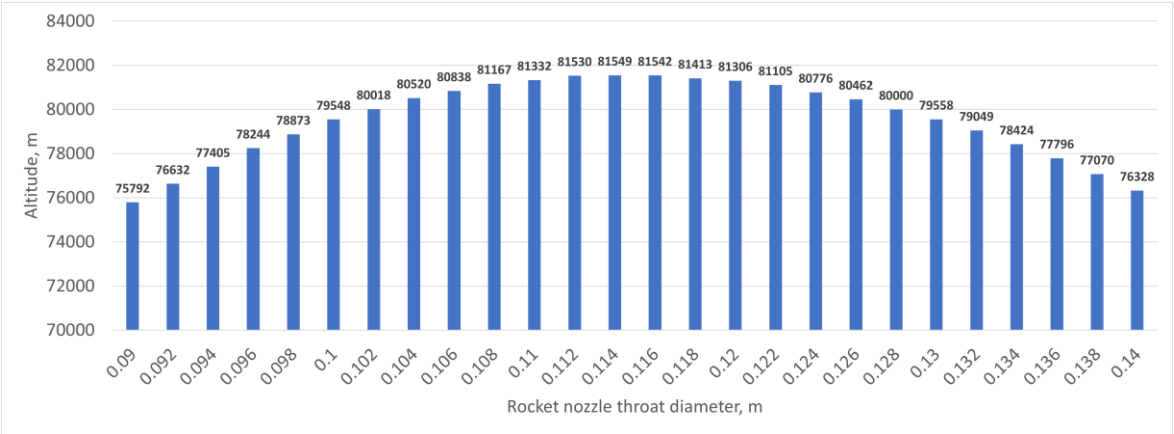

Figure 8.1. Evolution of the maximum altitude reached by the rocket with rocket nozzle throat diameter.

This shows that the ideal diameter for the nozzle throat for maximum performance is around 0.114 m.

8.2. Effects of Payload Mass in Flight Performance

After finding the ideal nozzle throat diameter, it can now be fixed as 0.114 m to analyze the maximum altitude reached by the rocket depending on the payload that it carries. For this analysis, simulations with the payload changing from 50 kg to 150 kg, in increments of 5 kg, will be made by the program.

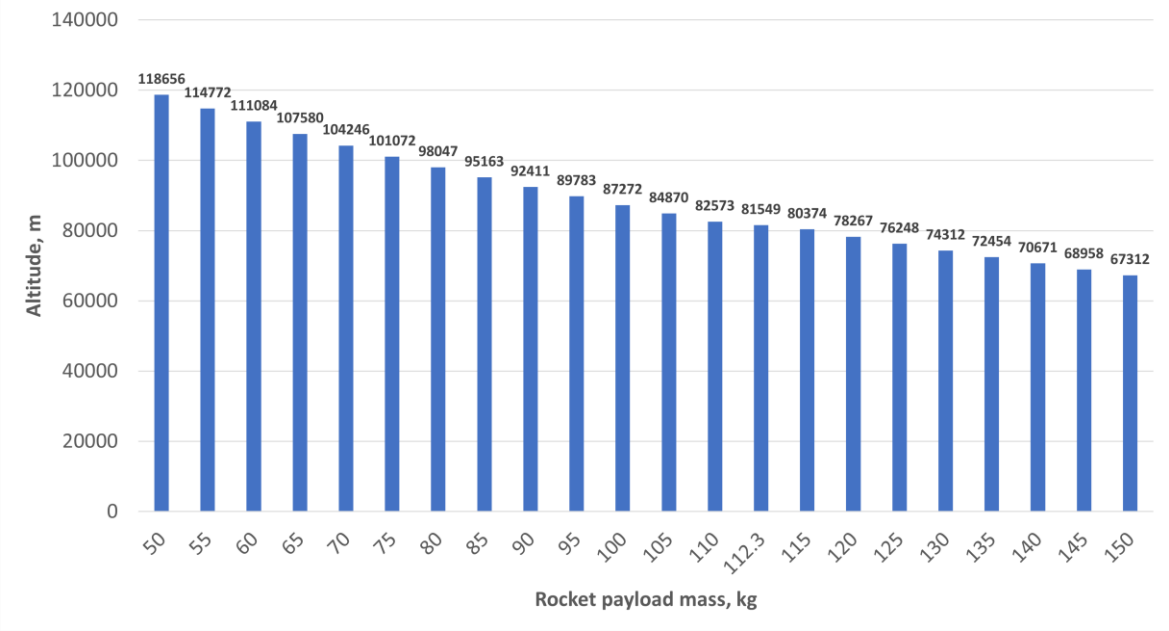

Figure 8.2. Evolution of the maximum altitude reached by the rocket with the payload.

As shown in the image, the rocket's maximum altitude, which depends on the payload it carries, can vary significantly within the chosen range of analysis. It ranges from 67312 meters when carrying a 150 kg payload to 118656 meters when carrying a 50 kg payload.

This shows a big impact of payload mass in the rocket apogee altitude.

8.3. Analysis of the Graphical Data Obtained Through MATLAB

In Figure 8.3, the geometrical height as a function of time is presented, with the rocket reaching its apogee of 81549 meters after 137.5 seconds and having a total flight duration of 278.2 seconds.

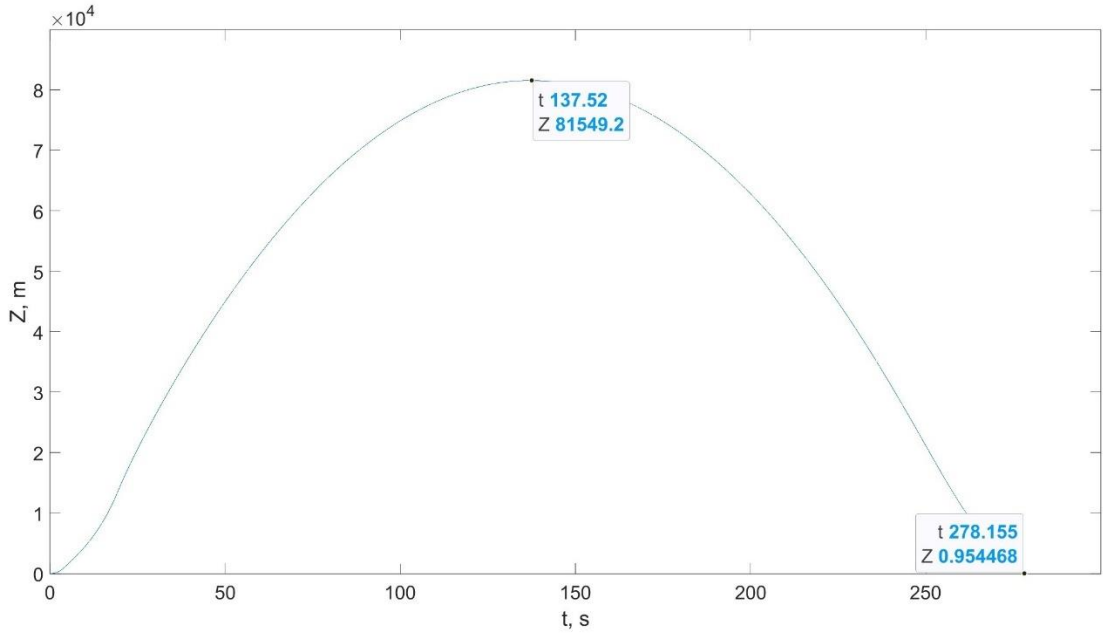

Figure 8.3. Geometrical height as a function of time.

In Figure 8.4, the rocket's acceleration as a function of time is presented. Here, we can see that the rocket reached a peak acceleration of 211.2 m/s², which translates to 21.5 g, with a total time of flight in microgravity conditions of around 180 seconds.

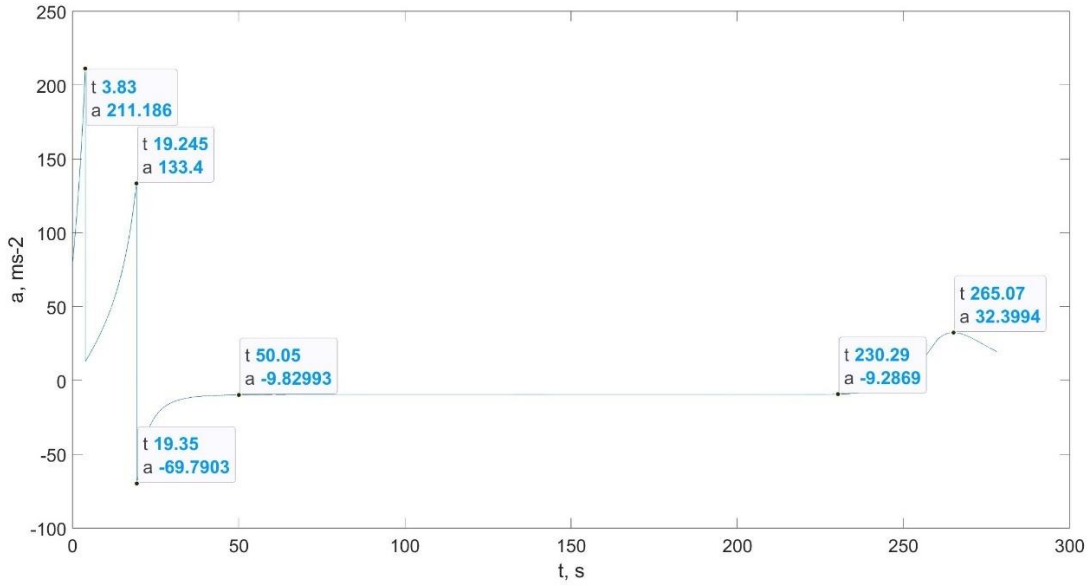

Figure 8.4. Acceleration as a function of time.

In Figure 8.5, the rocket's velocity as a function of time is presented. Here, we can see that the rocket reached a peak velocity of 1388.1 m/s after 19.3 seconds, which is the time that the burning of the propellant stopped.

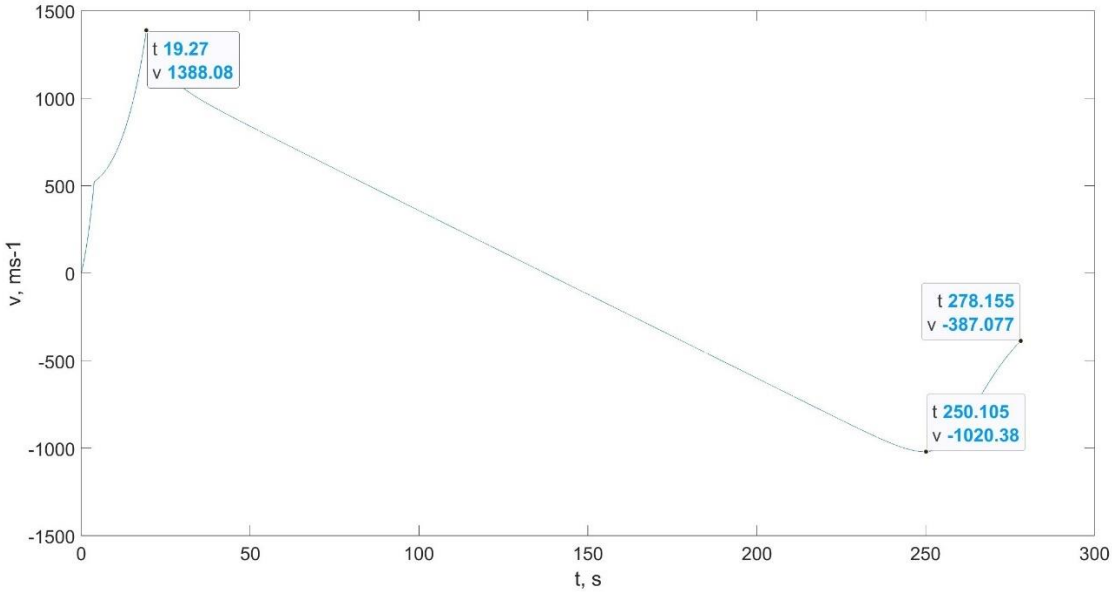

Figure 8.5. Velocity as a function of time.

In Figure 8.6, the Mach number as a function of time is presented. Here, we can see that it reached its peak of 4.7 after 19.3 seconds of flight time.

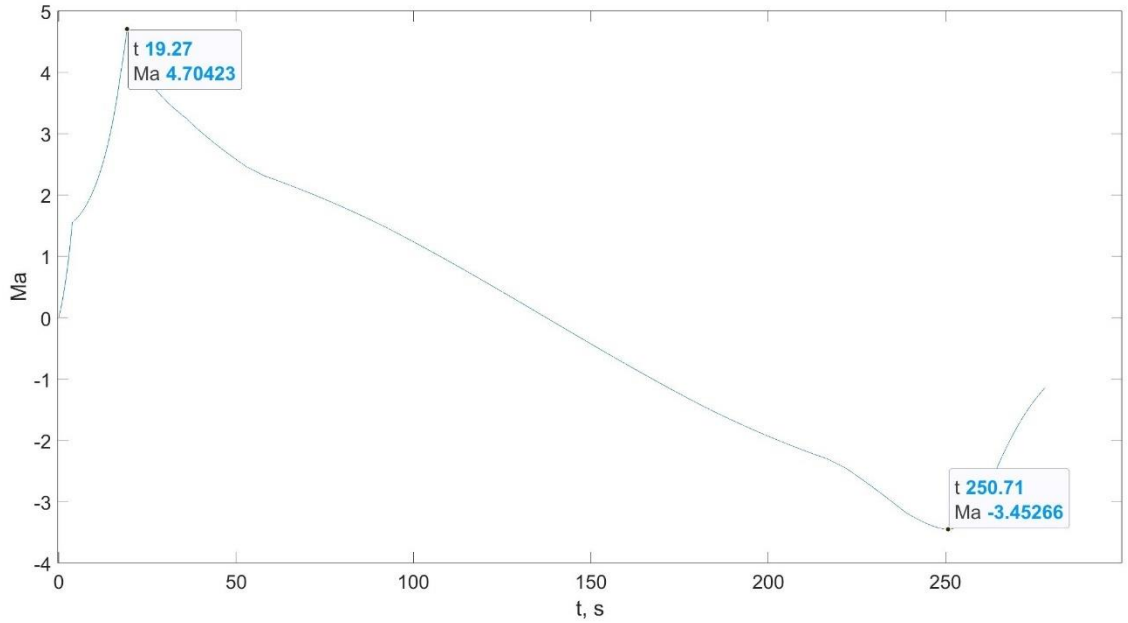

Figure 8.6. Mach number as a function of time.

In Figure 8.7, the rocket motor chamber pressure as a function of time is presented. Here, we can see that its peak pressure reaches 56.6 bar after 3.8 seconds of flight.

The slope seen in the graph is due to the increase in burning area diameter as propellant is burned, which makes the burning area of the propellant rise, thereby elevating the chamber pressure. The drop in chamber pressure at the 3.8 second mark is due to the end of propellant 1 burning and the start of propellant 2 burning. The propellant 2 stops burning at 19.3 seconds of flight time.

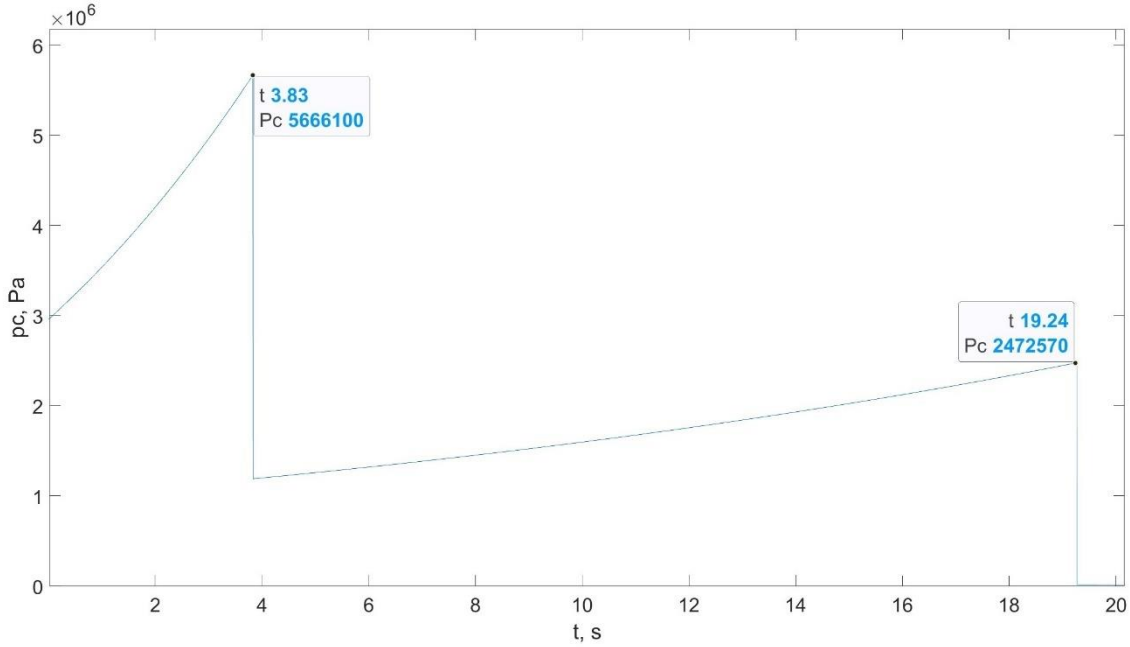

Figure 8.7. Rocket motor chamber pressure as a function of time.

9. CONCLUSIONS

Firstly, we were able to optimize the flight performance through changes in the rocket nozzle throat diameter and used this to simulate the optimized performance of this rocket while carrying 112.3 kg of payload mass.

Then, we confirmed the importance of reducing as much as possible the payload mass, being that it has a big impact in the rocket's achieved apogee altitude.

The Rexus-10 experiment achieved 82 km of maximum altitude with a payload of 112.3 kg and our simulation returned an apogee altitude of 81.5 km with the same payload.

The flight time to the apogee experimentally obtained was around 144 seconds, while the simulations returned a flight time to the apogee of 137.5 seconds.

The maximum acceleration of the Rexus-10 experiment was 21 g, while our simulation returns a maximum acceleration of 21.5 g.

The experimental data on this Rexus-10 mission refers to 180 seconds of flight in microgravity conditions, while our simulation returned a time of flight under microgravity conditions of around 180 seconds.

The pressure calculated in the rocket motor chamber can be used as a reference when designing the rocket motor structure.

Since the simulations results so closely resemble the results experimentally obtained, they serve as a confirmation for the model used in the MATLAB program created to perform the flight simulations.

REFERENCES

[1] Biblarz, O., & P. Sutton, G. (2017). *Rocket Propulsion Elements.* John Wiley & Sons.

[2] Dabrowski, A., Pelzner, K., Krawczuk, S., & Goczkowski, J. (2020). Acta Atronautica. *Acta Astronautica*.

[3] ESA. (2011, February 28). *Student experiments flown on REXUS 9 and 10*. Retrieved from ESA: https://www.esa.int/Education/Student_experiments_flown_on_REXUS_9_and_10

[4] Gordon, S., & McBride, B. J. (1994). *Computer Program for Calculation of Complex Chemical Equilibrium Compositions and Applications, I. Analysis, NASA RP-1311*. Cleveland, Ohio: NASA Lewis Research Center.

[5] Hoerner, S. F. (1965). *Fluid-Dynamic Drag.* Sighard F. Hoerner.

[6] ISO. (1975). *International Standard ISO 2533.* International Organization for Standardization.

[7] Lide, D. R., & Haynes, W. M. (2016-2017). *CRC Handbook of Chemistry and Physics.* Taylor and Francis Group LLC.

[8] *Newton's method*. (2023). Retrieved from Wikipedia: https://en.wikipedia.org/wiki/Newton%27s_method

[9] NOAA, NASA, & USAF. (1976). *U. S. Standard Atmosphere.* NOAA, NASA, USAF.

[10] Park, S., Choi, S., Kim, W., Kim, K., & Park, J. (2020). Effects of Ammonium Perchlorate Particle Size, Ratio, and. *Propellants, Explosives, Pyrotechnics*.

[11] *Polynomial interpolation*. (2023). Retrieved from Wikipedia: https://en.wikipedia.org/wiki/Polynomial_interpolation

[12] *REXUS 10*. (2011, May 13). Retrieved from sscspace: https://sscspace.com/rexus-10/

[13] S. Isert, L. Xin, J. Xie, & S.F. Son. (2017). Combustion and Flame. *Combustion and Flame*.

[14] Schüttauf, K. (2017). *Rexus User Manual.* EuroLaunch.

[15] Snyder, C. (2020, 10 29). *NASA Thermo Build*. Retrieved from https://cearun.grc.nasa.gov/ThermoBuild/index_ds.html

[16] *Sounding rockets*. (2023). Retrieved from ESA: https://www.esa.int/Science_Exploration/Human_and_Robotic_Exploration/Research/Sounding_rockets

[17] White, F. (2017). *Fluid Mechanics.* McGraw-Hill Education.